Supplementary Information

Interfacial perfluorosulfonic acid ionomer stabilizing sputtered Bi catalyst for highly selective and scalable CO_2-to-formate electroreduction

Chuyao Jin[1], Taoning Lei[1], Shaorui Zhang[2], Li Xu[1], Chen Yu[1], Na Li[3], Saisai Lin[1], Tao Wang[1], Jingjie Wang[2], Chenghang Zheng[1,3,4], Xiao Zhang[1,3,4,*], Xiang Gao[1,*]

[1]State Key Laboratory of Clean Energy Utilization, Zhejiang University, Hangzhou, 310027, China

[2]Harbin Boiler Co., Ltd., Harbin, 150046, China

[3]Zhejiang Baima Lake Laboratory Co., Ltd, Hangzhou, 310051, Zhejiang, China

[4]Jiaxing Research Institute, Zhejiang Key Laboratory of Clean Energy Conversion and Utilization, Zhejiang University, Jiaxing, 314000, China

[*]Email: xgao1@zju.edu.cn (X.Gao); zhangx_energy@zju.edu.cn (X.Zhang)

1 Materials

Bismuth target (Bi, φ50.8×4mm, 99.99%, Hebei JiuYue Advanced Material Technology Co., Ltd), carbon paper (YLS30T, Sinero), potassium chloride (KCl, ACS reagent, 99.0-100.5%, Sigma-Aldrich), sodium bicarbonate ($NaHCO_3$, ≥ 99.8%, Macklin), potassium bicarbonate ($KHCO_3$, ACS reagent, 99.7%, powder, Sigma-Aldrich), cesium hydrogen carbonate ($CsHCO_3$, 99.99% trace metals basis, Macklin), 12-crown-4 ($C_8H_{16}O_4$, ≥ 98%, D&B), 18-crown-6 ($C_{12}H_{24}O_6$, battery grade, Suzhou Duoduo Chemical Technology Co., Ltd.), nitric acid (HNO_3, 65-70%, 99.999% metals basis, Alfa Aesar), potassium hydroxide (KOH, ACS reagent, ≥ 85%, Sigma-Aldrich), perfluorosulfonic acid resin solution (Nafion, 5 wt% in a mixture of lower aliphatic alcohols and water, Macklin) and polytetrafluoroethylene resin (PTFE, 60 wt%, Aladdin) were used as received without further purification. Ultrapure water with a resistivity of 18.2 MΩ•cm (Rephile) was used in the experiments.

2 Preparation of Bi@CP, Bi@CP/PFSA and Bi@CP/PTFE electrodes

Preparation of Bi@CP electrodes. The Bi@CP electrode was prepared by depositing a Bi layer onto carbon paper (CP, YLS30T) via magnetron sputtering (JCP350, Beijing Technol Science Co., Ltd). Prior to deposition, the CP substrate was fixed onto a rotating holder. The sputtering process was conducted under a base pressure of 1×10^{-4} Pa with an Ar flow rate of 8 sccm using a direct-current power supply. The sputtering power was set to 20 W, the rotation speed of the sample holder was maintained at 20 rpm, and the deposition time was 40 min. The Bi loading was determined gravimetrically by weighing the carbon paper substrate before and after magnetron sputtering. The loading was then calculated from the mass increase divided by the geometric electrode area. Unless otherwise specified, the electrodes used in the main text had a Bi loading of 0.73 mg cm^{-2}.

Preparation of Bi@CP/PFSA electrodes. Bi@CP/PFSA electrodes were prepared by drop-casting PFSA dispersion onto the surface of the Bi@CP electrode. PFSA dispersions with different mass fractions relative to the sputtered Bi loading (5, 10, 20, and 30 wt%) were applied and the resulting electrodes were denoted as

Bi@CP/PFSA-x, where x represents the PFSA mass percentage. After drop-casting, the electrodes were dried at 80°C to obtain the PFSA-modified electrodes.

Preparation of Bi@CP/PTFE electrodes. For comparison, the Bi@CP/PTFE electrode was fabricated by drop-casting a PTFE dispersion onto the Bi@CP electrode surface with a PTFE loading of 10 wt% relative to the sputtered Bi mass. The electrode was subsequently dried at 200 °C to yield the PTFE-modified electrode.

3 Materials characterizations

The morphology of the samples was analyzed by scanning electron microscopy (SEM, Sigma 300, ZEISS). Elemental distribution was examined using X-ray energy dispersive spectroscopy (EDS, X-max80, Oxford) coupled with the SEM. X-ray diffraction (XRD, SmartLab SE, Rigaku) was used for phase analysis. The types and chemical states of elements on the electrode surface were obtained by X-ray photoelectron spectroscopy (XPS, ESCALAB QXi, Thermo Fisher Scientific). N_2 adsorption-desorption measurements were conducted using a surface area and pore size analyzer (BET, ASAP 2460, Micromeritics) to determine the BET surface area and pore structure of the samples. CO_2 adsorption-desorption measurements were performed at 25 °C using the same adsorption analyzer to evaluate the CO_2 uptake capacity of the samples. The contact angles were measured using a contact angle measuring device (CA, Theta Lite, Biolin Scientific AB) at ambient temperature, with the probe liquid being 3.5 μl of water. All contact angle images were taken 5 s after the application of the liquid droplet on the surface of the samples. For the quantitative determination of the amount of Bi detached from the electrode into the electrolyte during CO_2RR, inductively coupled plasma optical emission spectroscopy (ICP-OES, Avio 200, Perkin Elmer) was employed.

4 Electrochemical Measurements

All electrochemical measurements were conducted in a flow cell using a standard three-electrode configuration, with the anode and cathode compartments separated by a Nafion 117 membrane. Electrochemical measurements were controlled using a CHI760E and a Princeton VersaSTAT 3F (for impedance and ECSA measurements). 2

M KCl solution saturated with CO_2 (pH = 5.8) and 2 M KOH solution were used as the catholyte and anolyte for electrochemical CO_2 reduction experiments. All potentials were measured against an Ag/AgCl reference electrode (filled with saturated KCl solution), and converted to a reversible hydrogen electrode (RHE) scale using the formula E (vs. RHE) = E (vs. Ag/AgCl) + 0.197 V + 0.0591 V × pH (25 ℃). The as-prepared Bi electrode and a graphite rod were used as working electrode and counter electrode, respectively. Solution resistance (R_s) was measured before and after each experiment to compensate for the electrolyte ohmic losses. Unless otherwise specified, all short-term flow-cell electrolysis tests were conducted for 30 min at each applied current density.

All the EIS measurements were performed at -0.7 V vs. Ag/AgCl with a frequency range from 1×10^6 Hz to 0.01 Hz and an AC amplitude of 10 mV. The resulting Nyquist plots were analyzed with Zview, where R_s and R_{ct} are the electrolyte resistance and the charge transfer resistance at the electrode-electrolyte interface.

5 Calculations of product Faradaic efficiencies

The gaseous products were detected by an online gas chromatography (GC, 9790Plus, FULI INSTRUMENTS) equipped with a thermal conductivity detector (TCD) and a flame ionization detector (FID). Argon (Hangzhou Jingong Materials Co., Ltd., 99.999%) was used as the GC carrier gas and the GC was calibrated with H_2, CO, CH_4, and C_2H_4. The FEs of gaseous products were calculated as:

$$FE\ (\%) = \frac{N \times m \times v \times p \times F}{i \times R \times T} \times 100\%$$

where N is the number of electrons transferred per molecule of product (for H_2 and CO, N = 2), m is the volume fraction of the gaseous product, ν is the CO_2 feed flow rate (assumed to be equal to the outlet flow rate, at standard conditions), p is the standard pressure, F is the Faraday's constant, i is the current, R is the ideal gas constant, and T is the standard temperature.

Anionic liquid products were quantified by analyzing the collected catholyte using an ion chromatography (CIC-D160+, SHINE). Formate is the only product from CO_2RR detected by IC. Potassium formate standard solutions were used to obtain the

working curve of formate. The $FE_{formate}$ was calculated using the following formula:

$$FE\ (\%) = \frac{N \times c \times V \times F}{Q} \times 100\%$$

where N is the electron transfer number for product (for formate, N = 2), c is the measured concentration of formate, V is the volume of catholyte, F is the Faraday's constant, and Q is the total passed charge during reaction.

Nuclear magnetic resonance (NMR, DD2-600, Agilent) spectroscopy was used to examine the catholyte in the water suppression mode to detect any other CO_2RR product in the liquid phase. A known concentration of dimethyl sulfoxide (DMSO) was used as an internal standard. Only formate and DMSO signals were observed from the NMR spectra, confirming the feasibility of liquid product quantification with IC.

6 Supplementary Figures

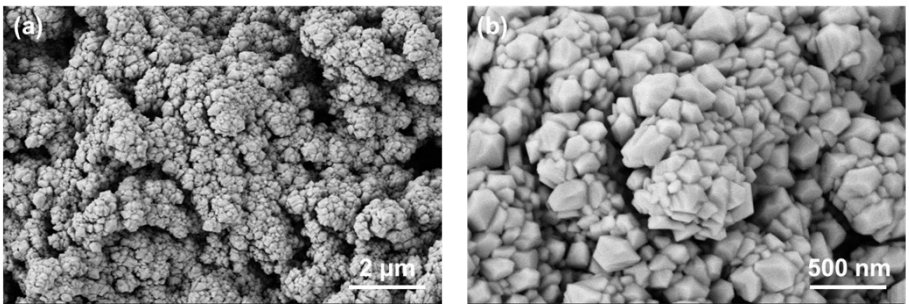

Fig. S1 SEM images of Bi@CP electrode at (a) low and (b) high magnification.

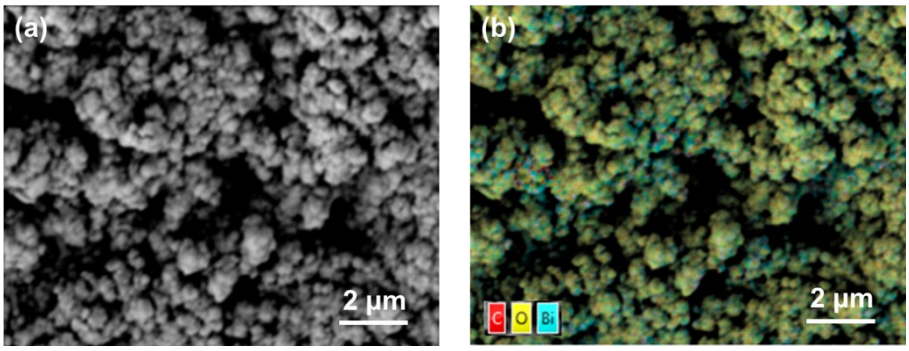

Fig. S2 Elemental mapping of Bi@CP electrode. (a) SEM image of Bi@CP. (b) EDS elemental map of Bi@CP.

118

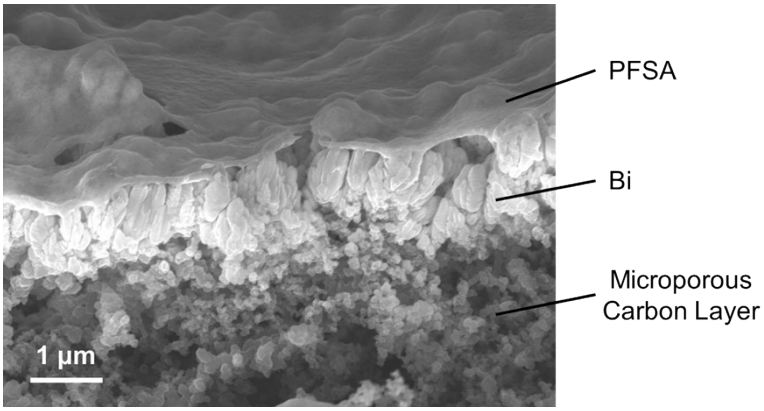

Fig. S3 Cross section SEM image of Bi@CP/PFSA.

119

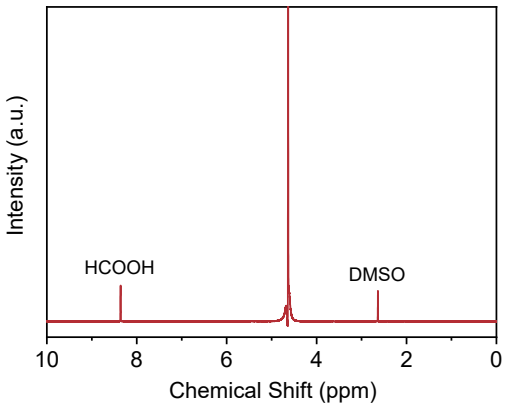

Fig. S4 Representative ^{1}H-NMR spectroscopy of catholyte after CO_2RR with Bi catalysts.

120

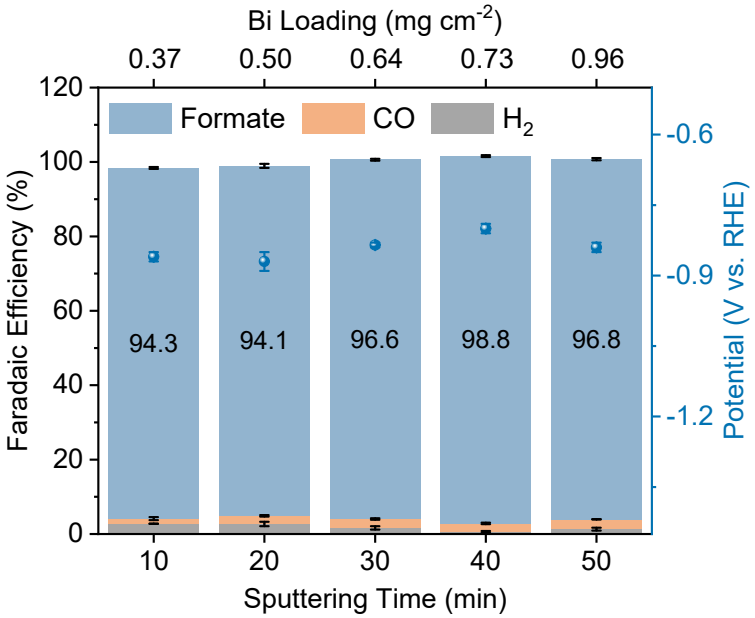

Fig. S5 Product distribution and reaction potential for Bi@CP with different Bi loadings in 2 M KCl solution at 150 mA cm^{-2}.

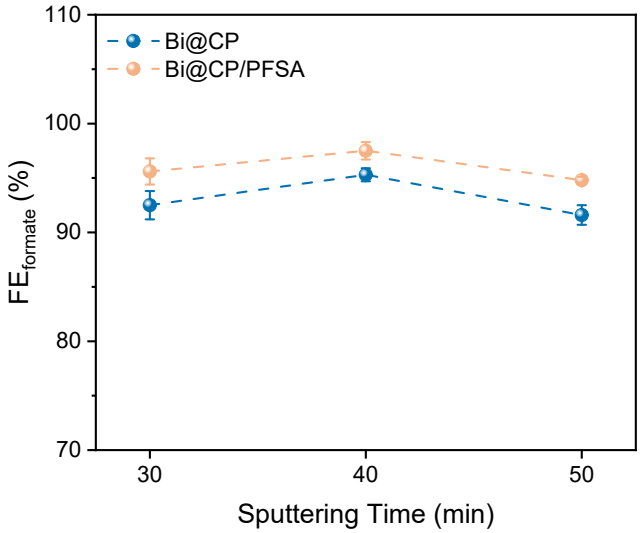

Fig. S6 $FE_{formate}$ for Bi@CP and Bi@CP/PFSA with different Bi loadings in 2 M KCl solution at 250 mA cm^{-2}.

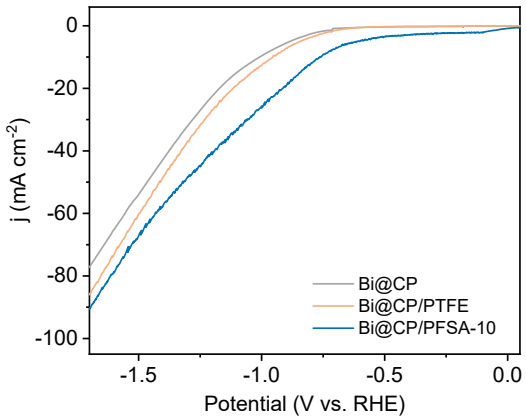

Fig. S7 Linear sweep voltammetry (LSV) comparison of different electrodes.

123

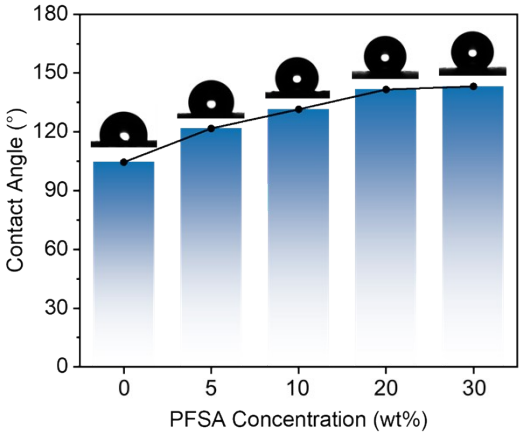

Fig. S8 Water contact angle of (a) Bi@CP, (b) Bi@CP/PFSA-5, (c) Bi@CP/PFSA-10, (d) Bi@CP/PFSA-20 and (e) Bi@CP/PFSA-30.

124

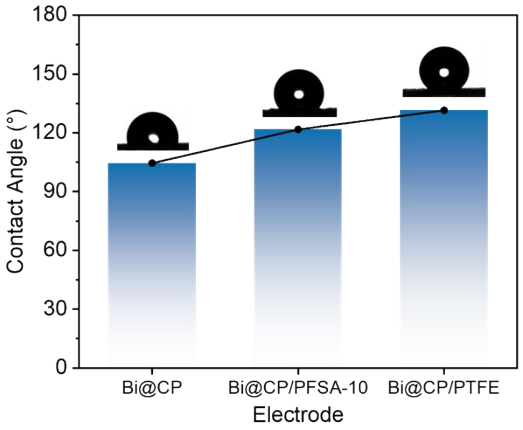

Fig. S9 Water contact angle of (a) Bi@CP, (b) Bi@CP/PFSA-10 and (c) Bi@CP/PTFE.

125

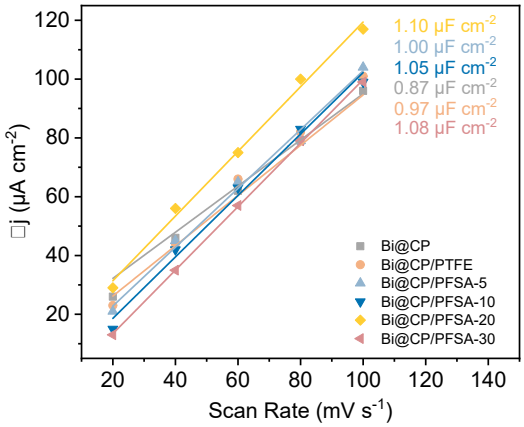

Fig. S10 Electrochemically active surface area (ECSA) comparison of different electrodes.

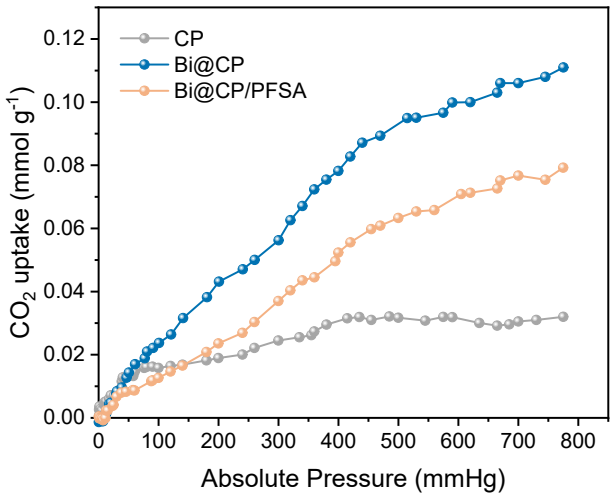

Fig. S11 CO_2 adsorption isotherms of CP, Bi@CP and Bi@CP/PFSA at 25 ℃.

127

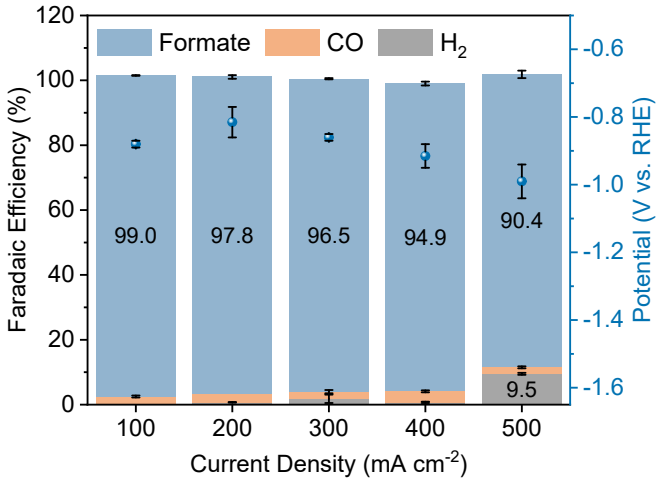

Fig. S12 Product distribution and reaction potential at different current densities for Bi@CP/PFSA-10 in 2 M KCl solution.

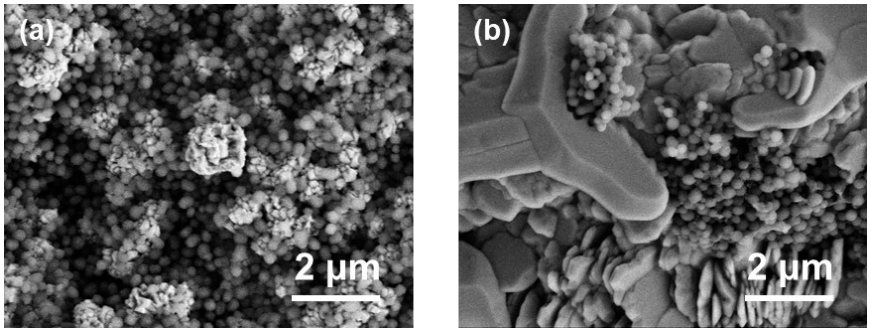

Fig. S13 SEM images of Bi@CP/PTFE (a) before and (b) after CO_2RR.

129

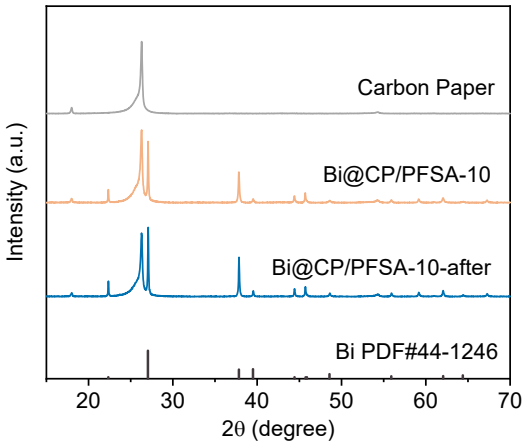

Fig. S14 XRD patterns of Bi@CP/PFSA-10 before and after electrolysis.

130

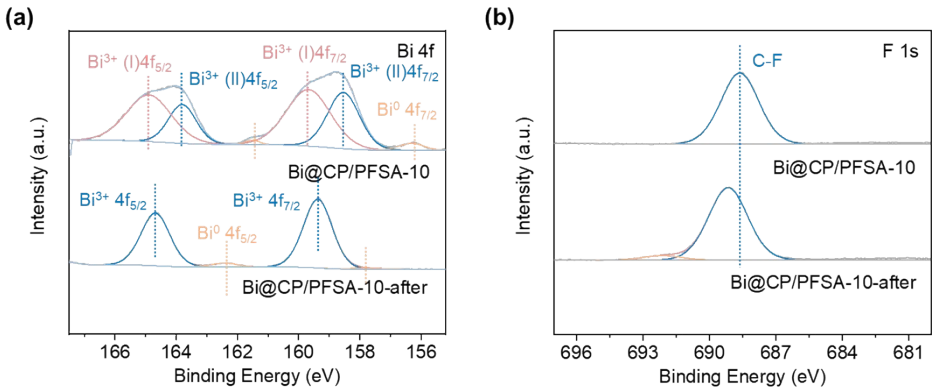

Fig. S15 Surface chemical evolution of Bi@CP/PFSA-10 during early-stage electrolysis. (a) Bi 4f XPS spectra before and after short-term electrolysis. (b) F 1s XPS spectra before and after short-term electrolysis.

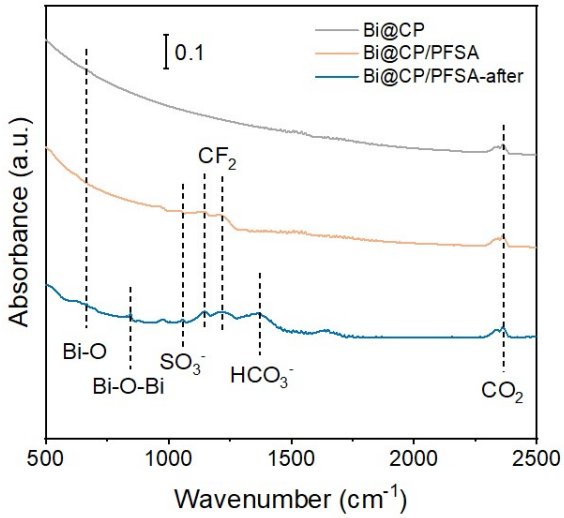

Fig. S16 Ex situ FTIR spectra of Bi@CP, Bi@CP/PFSA, and Bi@CP/PFSA after electrolysis.

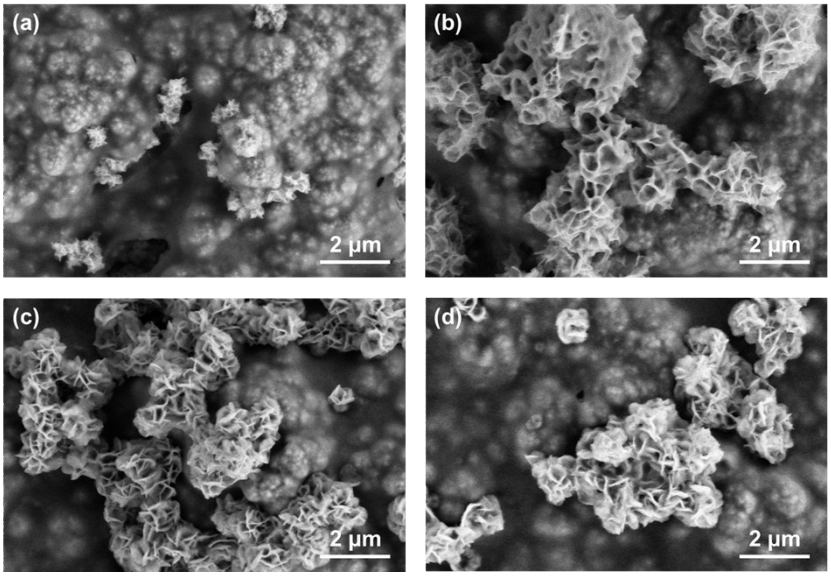

Fig. S17 SEM images of Bi@CP/PFSA-10 after electrolysis at (a) 100 mA cm^{-2}, (b) 200 mA cm^{-2}, (c) 300 mA cm^{-2} and (d) 400 mA cm^{-2}.

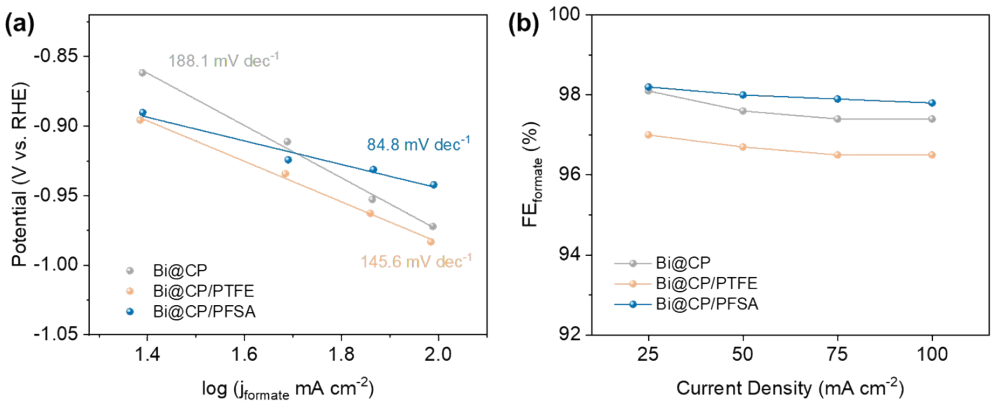

Fig. S18 Tafel analysis of Bi@CP, Bi@CP/PTFE, and Bi@CP/PFSA based on the formate partial current density. (a) Tafel plots constructed from the iR-corrected cathodic potential vs. log($j_{formate}$) for Bi@CP, Bi@CP/PTFE, and Bi@CP/PFSA. (b) $FE_{formate}$ of Bi@CP, Bi@CP/PTFE, and Bi@CP/PFSA at the current densities used for Tafel analysis.

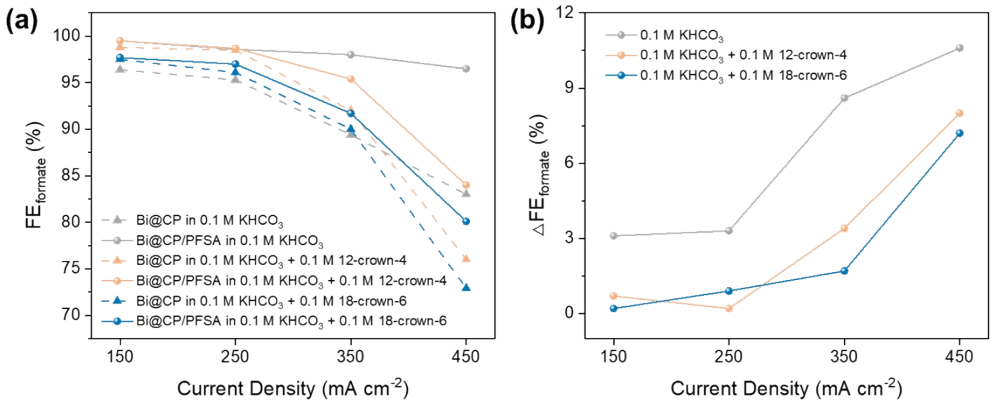

Fig. S19 Crown ether chelation experiments for evaluating the cation-related role of PFSA in CO_2RR. (a) $FE_{formate}$ and (b) PFSA-induced increment in $FE_{formate}$ ($\triangle FE_{formate}$) of Bi@CP and Bi@CP/PFSA under different electrolyte conditions at different current densities.

135

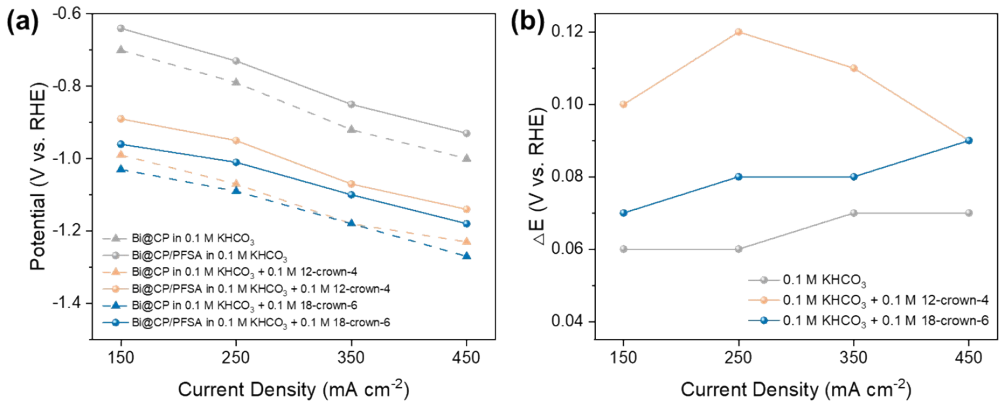

Fig. S20 Cathodic-potential analysis of crown ether chelation experiments for evaluating the cation-related role of PFSA in CO_2RR. (a) Cathodic potentials and (b) PFSA-induced increment in potential (△E) of Bi@CP and Bi@CP/PFSA under different electrolyte conditions at different current densities.

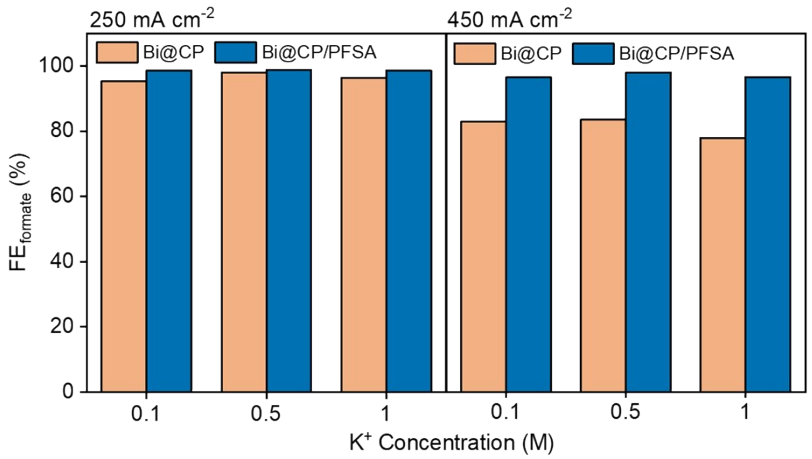

Fig. S21 CO_2RR performance of Bi@CP and Bi@CP/PFSA in $KHCO_3$ electrolytes with different K^+ concentrations at different current densities.

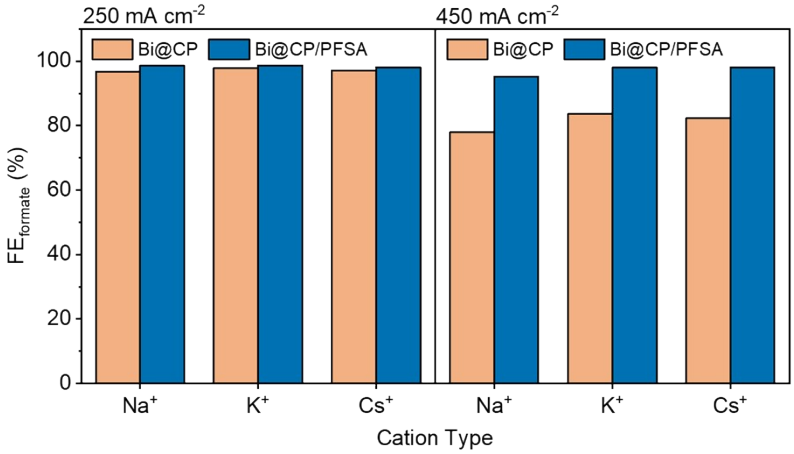

Fig. S22 CO_2RR performance of Bi@CP and Bi@CP/PFSA in 0.5 M $NaHCO_3$, $KHCO_3$ and $CsHCO_3$ electrolytes at different current densities.

Table S1

Textural parameters of CP, Bi@CP/PFSA, and Bi@CP derived from N_2 adsorption measurements.

Catalyst	BET surface area ($m^2\ g^{-1}$)	Single-point total pore volume ($cm^3\ g^{-1}$)
CP	1.4475	0.000149
Bi@CP/PFSA	4.8261	0.005395
Bi@CP	5.5632	0.006943

Table S2

CO_2 uptake values at representative pressures for CP, Bi@CP and Bi@CP/PFSA at 25 ℃.

Pressure (mmHg)	CP (mmol g^{-1})	Bi@CP (mmol g^{-1})	Bi@CP/PFSA (mmol g^{-1})
50	0.0130	0.0141	0.0085
100	0.0158	0.0236	0.0127
200	0.0190	0.0430	0.0236
400	0.0307	0.0783	0.0524
760	0.0272	0.1087	0.0773

Table S3

Summary of formate production from CO_2RR over various Bi based electrodes in a flow cell.

Number	Catalysts	Electrolyte	Potential	$FE_{formate}$ (%)	Current density (mA cm^{-2})	Time (h)	Electrode area (cm^2)	Ref.
1	Bi@CP/PFSA	2M KCl	-1.0V vs. RHE	94.9	400	0.5	1	This work
2	Bi@CP/PFSA	2M KCl	/	93.0	100	135	25	This work
3	Bi@CP/PFSA	2M KCl	/	94.0	250	95	25	This work
4	syn-Bi_2O_3	1M KOH	-0.7V vs. RHE	94.0	100	28	1	[1]
5	GB-Bi	1M KOH	-0.5V vs. RHE	90.0	100	122	1	[2]
6	CT/h-BiOBr	1M KOH	-0.9V vs. RHE	96.0	165	18	1	[3]
7	Bi-NC	1M KOH	-1.0V vs. RHE	92.0	100	45	1	[4]
8	$BiFeO_3/Bi_{25}FeO_{40}$	1M KOH	-0.64V vs. RHE	95.0	140	88	1	[5]
9	f-Bi_2O_3/CF	0.5M $KHCO_3$	-1.1V vs. RHE	85.0	180	20	1	[6]
10	O_V-Bi	1M KOH	/	93.0	500	/	5	[7]
11	BND-ZIF8	0.5M $KHCO_3$	-1.1V vs. RHE	80.0	110	24	1	[8]
12	$Bi_{24}O_{31}Cl_{10}$	1M KOH	-1.2V vs. RHE	99.1	600	/	1	[9]
13	$Bi_{1,n}$-pBi_2O_{3-x}	0.5M $KHCO_3$	-1.0V vs. RHE	90.0	20	150	1	[10]

Table S4

Concentrations of dissolved Bi in the electrolytes after CO_2RR measured by ICP-OES.

Catalyst	Concentration (ppb)
Bi@CP	482.3
Bi@CP/PFSA-10	58.0

Table S5

The EIS fitting results of different Bi catalysts at -0.7 V vs. Ag/AgCl in CO_2-saturated atmosphere.

Catalyst	R_s (Ω)	R_{ct} (Ω)
Bi@CP	3.58	115.30
Bi@CP/PTFE	3.57	170.40
Bi@CP/PFSA-10	3.42	67.69

Table S6

Cathodic potentials of Bi@CP and Bi@CP/PFSA in $KHCO_3$ electrolytes with different concentrations.

Catalyst	Electrolyte	Current density ($mA\ cm^{-2}$)	Potential (V vs. RHE)
Bi@CP	0.1 M $KHCO_3$	250	-0.79
Bi@CP/PFSA-10			-0.73
Bi@CP	0.5 M $KHCO_3$		-0.75
Bi@CP/PFSA-10			-0.72
Bi@CP	1 M $KHCO_3$		-0.70
Bi@CP/PFSA-10			-0.68
Bi@CP	0.1 M $KHCO_3$	450	-1.00
Bi@CP/PFSA-10			-0.93
Bi@CP	0.5 M $KHCO_3$		-0.97
Bi@CP/PFSA-10			-0.92
Bi@CP	1 M $KHCO_3$		-0.88
Bi@CP/PFSA-10			-0.87

Table S7

Cathodic potentials of Bi@CP and Bi@CP/PFSA in 0.5 M $NaHCO_3$, $KHCO_3$ and $CsHCO_3$ electrolytes.

Catalyst	Electrolyte	Current density (mA cm^{-2})	Potential (V vs. RHE)
Bi@CP	0.5 M $NaHCO_3$	250	-0.79
Bi@CP/PFSA-10			-0.75
Bi@CP	0.5 M $KHCO_3$		-0.75
Bi@CP/PFSA-10			-0.72
Bi@CP	0.5 M $CsHCO_3$		-0.76
Bi@CP/PFSA-10			-0.72
Bi@CP	0.5 M $NaHCO_3$	450	-1.01
Bi@CP/PFSA-10			-0.93
Bi@CP	0.5 M $KHCO_3$		-0.97
Bi@CP/PFSA-10			-0.92
Bi@CP	0.5 M $CsHCO_3$		-0.99
Bi@CP/PFSA-10			-0.95

7 Reference

1 D. Lei, Y. Ren, G. He, T. Ma, C. Liao, S. Bai, F. Wang, Y. Liu, L. Guo. *Small,* 2026, **22**, e12691.

2 L. Luo, Q. Gao, H. Wang, C. Liu, Y. Ji, X. Li, Q. Jiang, T. Zheng, C. Xia. *Nano Letters,* 2025, **25**, 13918-13925.

3 Y. Chen, Y. Zhang, Z. Li, M. Liu, Q. Wu, T. W. B. Lo, Z. Hu, L. Y. S. Lee. *ACS Nano,* 2024, **18**, 19345-19353.

4 C. Weng, C. Wang, Y. Song, Y.-X. Zhang, K. Zou, H. Chen, X. Yang, W. Lin. *Chemical Engineering Journal,* 2025, **505**, 159732.

5 C. Xu, Y. Wang, W. Li, D. Gao, G. Wang, R. Cai. *ACS Applied Materials & Interfaces,* 2024, **16**, 39305-39311.

6 M. Wang, Y. Gu, J. Li, H. Wang, M. Zhu, J. Liang, Z. Tie, J. Ma, Z. Jin. *Nano Energy,* 2024, **126**, 109659.

7 J. Jeon, H.-S. Bang, Y.-J. Ko, E. Huh, J. Kang, X. Zhang, S. Ka, Y. Kim, W. H. Lee, K. Kim, H. K. Yu, H.-S. Oh, J.-Y. Choi. *Chemical Engineering Journal,* 2025, **523**, 168350.

8 M. Usman, M. H. Suliman, M. Abdinejad, J. Kok, H. A. Naji, A. Helal, Z. H. Yamani, G. Centi. *Carbon Capture Science & Technology,* 2025, **16**, 100450.

9 J. Wu, J. Ge, S. Zhao, Y. Ji, Y. Li, S. Kim, Y. Choi, Y. Namgung, H. E. Lee, H. O. Seo, T. Li, W. Zhang, Z. Peng, Z. Liu, Y. D. Kim. *Chemical Engineering Journal,* 2026, **528**, 172328.

10 M. Zhang, W. Zhu, Z. Liu, S. Chen, D. Zhou, X. Mu, Z. Zhuang, S. Wang, J. Yang, Y. Du, X. Luo, Q. Zhang, S. Liu, D. Wang, Z. Dai. *Angewandte Chemie International Edition,* 2025, **64**, e202510206.